AGU PUBLICATIONS

Geophysical Research Letters

RESEARCH LETTER
10.1002/2014GL061904

Key Points:
- A new Earth's gravity field model from the entire GOCE mission is presented
- GOCE data are converted to a user-friendly product with quality description
- The processing and use of GOCE-only data allow the usage in many applications

Correspondence to:
J. M. Brockmann,
brockmann@geod.uni-bonn.de

Citation:
Brockmann, J. M., N. Zehentner, E. Höck, R. Pail, I. Loth, T. Mayer-Gürr, and W.-D. Schuh (2014), EGM_TIM_RL05: An independent geoid with centimeter accuracy purely based on the GOCE mission, *Geophys. Res. Lett.*, *41*, 8089–8099, doi:10.1002/2014GL061904.

Received 17 SEP 2014
Accepted 03 NOV 2014
Accepted article online 6 NOV 2014
Published online 25 NOV 2014

EGM_TIM_RL05: An independent geoid with centimeter accuracy purely based on the GOCE mission

Jan Martin Brockmann[1], Norbert Zehentner[2], Eduard Höck[2,3], Roland Pail[4], Ina Loth[1], Torsten Mayer-Gürr[2], and Wolf-Dieter Schuh[1]

[1]Institute of Geodesy and Geoinformation, Department of Theoretical Geodesy, University of Bonn, Bonn, Germany, [2]Institute of Theoretical Geodesy and Satellite Geodesy, Graz University of Technology, Graz, Austria, [3]Space Research Institute, Austrian Academy of Sciences, Graz, Austria, [4]Institute for Astronomical and Physical Geodesy, Technische Universität München, Munich, Germany

Abstract After more than 4.5 years in orbit, the Gravity field and steady-state Ocean Circulation Explorer (GOCE) mission ended with the reentry of the satellite on 11 November 2013. This publication serves as a reference for the fifth gravity field model based on the time-wise approach (EGM_TIM_RL05), a global model only determined from GOCE observations. Due to its independence of any other gravity data, a consistent and homogeneous set of spherical harmonic coefficients up to degree and order 280 (corresponding to spatial resolution of 71.5 km on ground) is provided including a full covariance matrix characterizing the uncertainties of the model. The associated covariance matrix realistically describes the model quality. It is the first model which is purely based on GOCE including all observations collected during the entire mission. The achieved mean global accuracy is 2.4 cm in terms of geoid heights and 0.7 mGal for gravity anomalies at a spatial resolution of 100 km.

1. Introduction

The Gravity field and steady-state Ocean Circulation Explorer (GOCE) satellite mission [*ESA*, 1999] was launched on 17 March 2009 as the first Earth Explorer of the European Space Agency's (ESA) Living Planet Programme [*ESA*, 1998]. The mission objective was to survey the static part of the Earth's gravity field with a global mean accuracy of 1 mGal for gravity anomalies or 2 cm for geoid heights, respectively, at a spatial resolution of 100 km. Although the entire satellite acts as the sensor [*Floberghagen et al.*, 2011], the core and unique measurement instrument is a three-axes gradiometer, measuring acceleration differences along baselines of 0.5 m in the gradiometer reference frame (GRF) defined by the orthogonal gradiometer arms [*EGG-C*, 2010, section 8.2]. These measurements—reduced by centrifugal terms and properly calibrated [see *Rummel et al.*, 2011; *Frommknecht et al.*, 2011; *Stummer et al.*, 2012]—are the second derivatives of the Earth's gravitational potential in the GRF. The onboard gradiometer records all six elements of the symmetric gravitational tensor. However, due to the engineering design, only four (V_{XX}, V_{YY}, V_{ZZ}, and V_{XZ}) of the six (V_{YZ} and V_{XY} are about 30 to 70 times more inaccurate) nonredundant components can be measured with sufficiently high precision in the so-called measurement band (MB) between 5×10^{-3} Hz and 0.1 Hz (10–20 mE/$\sqrt{\text{Hz}}$, [*Rummel et al.*, 2011]. Whereas the measurement noise is almost constant (i.e., white) within the MB, it rapidly increases for the smaller frequencies and shows a nonwhite $1/f$ characteristic [see, e.g., *Rummel et al.*, 2011; *Pail et al.*, 2011a; *Schuh et al.*, 2010]. This complex noise behavior requires a careful modeling to allow for an accurate derivation of the gravity field models and a realistic covariance matrix [*Schuh et al.*, 2010]. In addition to the gravity gradiometer, an onboard receiver tracks the satellites of the Global Positioning System (GPS) to compute the satellite position (1–2 cm accuracy). These positions are used first for the geolocation of the measured gravity gradients and second as observables for the long-wavelength components of the gravity field. The orientation of the satellite is determined by star trackers.

Various gravity field models based on GOCE observations have been published since the beginning of the mission. On the one hand, some of these models were determined by GOCE observations only. These pure GOCE models are the preceding releases of the time-wise series [*Pail et al.*, 2011a, 2011b; *Brockmann et al.*, 2013], the official ESA releases derived by the space-wise method [*Pail et al.*, 2011a; *Migliaccio et al.*, 2011], and the ITG-Goce02 model [*Schall et al.*, 2014]. JYY_GOCE02S [*Yi*, 2012; *Yi et al.*, 2013] is also a

GOCE-only model but contains external information concerning the polar areas. On the other hand, some combined gravity field models which include GOCE data are available. These either include observations from other satellites such as Challenging Minisatellite Payload [*Reigber et al.*, 2002], GRACE (Gravity Recovery and Climate Experiment) [*Tapley et al.*, 2004], satellites tracked by laser measurements (SLR), or they include additional terrestrial and altimetry observations. These are the official ESA models based on the direct approach [*Pail et al.*, 2011a; *Bruinsma et al.*, 2013, 2014] and the closely related EIGEN series, produced by the same team [*Förste et al.*, 2008; *Shako et al.*, 2014]. The EIGEN series contains a number of combined gravity field models (i.e., the EIGEN6C series). A satellite-only model, combining GRACE and GOCE observations was published by *Farahani et al.* [2013]. Additionally, the satellite-only models of the GOCO (http://www.goco.eu) series are available [*Pail et al.*, 2010; *Mayer-Gürr et al.*, 2012].

In this paper the fifth release of ESA's time-wise model (EGM_TIM_RL05) is presented. The model consists of a spherical harmonic (SH) series up to degree and order (d/o) 280 (representing a spatial resolution of 71.5 km on ground). Currently, the fifth release of the time-wise model is the first GOCE-only model based on the entire mission data set. In section 2 the used data and the estimation procedure are shortly summarized. Section 3 summarizes the characteristics of the new Release 5 solution EGM_TIM_RL05 via comparison with other global gravity field models which are independent of GOCE observations. The internal consistency is shown by comparing subsolutions of parts of the GOCE measurements to the final model. A comparison to the EGM2008 model highlights the additional new gravity information observed by the GOCE mission. It is shown that the associated covariance matrix is a realistic descriptor of the model quality. The final section 4 summarizes the results and provides some conclusions.

2. Used Methods and Used Data

The Earth's gravitational potential $V(r, \theta, \lambda)$ is typically parameterized as a finite series of SH base functions [e.g., *Heiskanen and Moritz*, 1993, p. 59], that is,

$$V(r,\theta,\lambda) = \frac{GM}{a}\sum_{l=0}^{l_{\max}}\left(\frac{a}{r}\right)^{l+1}\sum_{m=0}^{l}\left(c_{lm}\cos(m\lambda)+s_{lm}\sin(m\lambda)\right)P_{lm}(\cos\theta)\,. \tag{1}$$

l and m are the SH d/o, a is the equatorial radius of the Earth reference ellipsoid, GM the gravitational constant of the Earth, and $P_{lm}(\cdot)$ denote the fully normalized associated Legendre functions. c_{lm} and s_{lm} are the unknown SH coefficients to be estimated from the observations in a least squares adjustment.

2.1. Summary of the Time-wise Method

The time-wise method used here was already published in a number of papers [e.g., *Pail and Plank*, 2002; *Pail et al.*, 2006, 2011a, 2011b]. For that reason, only a short summary completed by detailed references is provided. Both observation types, i.e., the GPS satellite tracking observations (SST-hl) and the measured gravity gradients (SGG), were combined in a joint least squares adjustment, which additionally includes two groups of stochastic prior information in order to stabilize the inversion. The combined normal equations (NEQs) were then set up using the addition theorem for NEQs [*Koch*, 1999, p. 177], that is,

$$\begin{aligned}&\left(\sum_t \frac{1}{\sigma^2_{\mathrm{SST},t}}\mathbf{N}_{\mathrm{SST},t}+\sum_r \frac{1}{\sigma^2_{\mathrm{REG},r}}\mathbf{N}_{\mathrm{REG},r}+\sum_g \frac{1}{\sigma^2_{\mathrm{SGG},g}}\mathbf{N}_{\mathrm{SGG},g}\right)\mathbf{x}\\ &=\sum_t \frac{1}{\sigma^2_{\mathrm{SST},t}}\mathbf{n}_{\mathrm{SST},t}+\sum_r \frac{1}{\sigma^2_{\mathrm{REG},r}}\mathbf{n}_{\mathrm{REG},r}+\sum_g \frac{1}{\sigma^2_{\mathrm{SGG},g}}\mathbf{n}_{\mathrm{SGG},g},\end{aligned} \tag{2}$$

$$\mathbf{N}\mathbf{x}=\mathbf{n}. \tag{3}$$

These NEQs were then solved for the unknown parameters $\mathbf{x}$, containing the SH parameters c_{nm} and s_{nm}. The individual weights $w_i = \frac{1}{\sigma_i^2}$ were iteratively determined using variance component estimation (VCE) [*Koch and Kusche*, 2002]. An in-core Cholesky decomposition was used to solve for the parameters, and its full covariance matrix $\mathbf{\Sigma_{xx}} = \mathbf{N}^{-1}$ was determined.

2.1.1. Processing of the GPS Positions

The observed satellite positions were used to estimate the long-wavelength gravity field. In this context it is of crucial importance for the processing of the satellite orbit that the positions are estimated epoch by epoch only on the basis of the geometrical observations, i.e., without using any a priori force model (kinematic orbit). The orbit used in the processing of the EGM_TIM_RL05 model was computed at the Institute of Theoretical Geodesy and Satellite Geodesy at Graz University of Technology on the basis of a Precise Point Positioning (PPP) approach [e.g., *Witchayangkoon*, 2000]. The main difference in comparison to other methods is the fact that observations were used directly within the least squares adjustment, without forming any linear combinations or differences. This comprises phase as well as code observations on both available GPS carrier frequencies. Different influences on GPS observations were considered, as there are transmitter orbits and clocks, phase center offsets, antenna center variations, phase wind-up, relativistic effects, code biases, and ionospheric refraction. The transmitter orbit and clock products were taken from the Center for Orbit Determination in Europe (CODE) [*Dach et al.*, 2009], which provides clock information sampled with 5 s. Ionospheric refraction was taken into account by estimating the Slant Total Electron Content (STEC) for each observed transmitter at each epoch. The parameterization of the STEC included first-, second-, and third-order terms [*Fritsche et al.*, 2005]. The observations were corrected for the bending effect [*Hoque and Jakowski*, 2008]. Antenna phase center variations were estimated beforehand for the receiver as well as the transmitters in two successive iterations. The approach was presented in *Zehentner and Mayer-Gürr* [2012, 2013, 2014]. The produced kinematic orbits along with epochwise covariance information served as input for the gravity field estimation. To account for interepoch correlations, an empirical covariance function was used to realistically describe the stochastic behavior of the kinematic orbit positions. There are different methods to exploit the gravity information contained in kinematic orbits (for GOCE real data, see *Baur et al.* [2014]). For the EGM_TIM_RL05 gravity field, the short arc integral equation method (as refined by *Mayer-Gürr* [2006]) was used. This approach was applied successfully to produce the series of the ITG-Grace gravity field models (and now followed by ITSG-Grace models *Mayer-Gürr et al.* [2010a, 2010b]). The kinematic orbit was split into short arcs of a few minutes up to a few hours. This leads to the formulation as a boundary value problem. The NEQs for the least squares adjustment were set up for each arc individually and then accumulated over the whole period. For every arc, data adaptive weights were estimated with VCE. The used arc length was 35 min, and several arc-specific parameters were eliminated. This gave one final normal equation matrix, which was combined with the SGG NEQs. For the EGM_TIM_RL05, these NEQs from the SST-hl observations were set up to d/o 150 (i.e., 22 797 parameters, 2 GB for a triangle of the symmetric matrix).

2.1.2. Processing of the Gradiometer Observations

This part briefly describes how the NEQs $\mathbf{N}_{\mathrm{SGG},g} = \mathbf{A}^T_{\mathrm{SGG},g}\mathbf{Q}^{-1}_{\boldsymbol{\ell}_g\boldsymbol{\ell}_g}\mathbf{A}_{\mathrm{SGG},g}$ for the SGG observations were set up. The subscript g indicates that several NEQs were set up individually (i) for each tensor component and (ii) for gapless segments of the time series. The SGG observations of every tensor component were handled as equidistant time series along the orbit.

The observation equations were set up in the GRF to avoid a rotation of the original SGG observations (for details, see *Hausleitner* [1995, section 4]). To account for the correlations, instead of the cofactor matrix $\mathbf{Q}_{\boldsymbol{\ell}_g\boldsymbol{\ell}_g}$, digital autoregressive moving average filters were used as whitening filters [*Schuh*, 1996, 2003; *Siemes*, 2008; *Krasbutter et al.*, 2011]. The observation equations were transformed with a data adaptive estimated filter, written symbolically as a matrix F_g, such that

$$\mathrm{F}_g\boldsymbol{\ell}_g + \mathrm{F}_g\mathbf{v}_g = \mathrm{F}_g\mathbf{A}_g\mathbf{x} \tag{4}$$

$$\Leftrightarrow \bar{\boldsymbol{\ell}}_g + \bar{\mathbf{v}}_g = \bar{\mathbf{A}}_g\mathbf{x}, \qquad \boldsymbol{\Sigma}_{\bar{\boldsymbol{\ell}}_g\bar{\boldsymbol{\ell}}_g} = \sigma_g^2\mathrm{F}_g\mathbf{Q}_{\boldsymbol{\ell}_g\boldsymbol{\ell}_g}\mathrm{F}_g^T \approx \sigma_g^2\mathbf{I}, \tag{5}$$

where $\boldsymbol{\ell}_g$ and $\mathbf{v}_g$ denote the vectors of observations and residuals of a single segment and gradient component. After filtering, the computation of the (partial) NEQs is straightforward although computationally demanding [*Plank*, 2004; *Pail and Plank*, 2002]. They were computed from

$$\mathbf{N}_{\mathrm{SGG},g} = \bar{\mathbf{A}}^T_{\mathrm{SGG},g}\bar{\mathbf{A}}_{\mathrm{SGG},g}, \tag{6}$$

$$\mathbf{n}_{\mathrm{SGG},g} = \bar{\mathbf{A}}^T_{\mathrm{SGG},g}\bar{\boldsymbol{\ell}}_{\mathrm{SGG},g}. \tag{7}$$

Table 1. Details of the Input to the Time-wise GOCE Gravity Field Models

Release/Type	Input/Information	Time Series	(d/o)	# Observations
EGM_TIM_RL01	SST, SGG, REG	11/2009–1/2010	2–224	24,524,268
SST	Energy balance, in-flight velocity	Pointwise	2–100	6,013,954
SGG	V_{XX}, V_{YY}, V_{ZZ}	1 gapless segment	2–224	$3 \times 6,161,834$
REG	Zonal coefficients	–	$m < \theta_0 l$	5,490
REG	High-degree coefficients	–	170–224	19,322
EGM_TIM_RL02	SST, SGG, REG	11/2009–7/2010	2–250	82,696,288
SST	Energy balance, in-flight velocity	Pointwise	2–100	24,228,376
SGG	V_{XX}, V_{YY}, V_{ZZ}	9 gapless segments	2–250	$3 \times 19,477,946$
REG	Zonal coefficients	–	$m < \theta_0 l$	6,866
REG	High-degree coefficients	–	180–250	27,208
EGM_TIM_RL03	SST, SGG, REG	11/2009–4/2011	2–250	$\approx 215,000,000$
SST	Energy balance, in-flight velocity	Pointwise	2–100	$\approx 3 \times 30,000,000$
SGG	$V_{XX}, V_{YY}, V_{ZZ}, V_{XZ}$	16 gapless segments	2–250	$4 \times 31,289,605$
REG	Zonal coefficients	–	$m < \theta_0 l$	6,866
REG	High-degree coefficients	–	180–250	27,208
EGM_TIM_RL04	SST, SGG, REG	11/2009–6/2012	2–250	480,719,445
SST	Short arcs, 3-D positions	35 min arcs	2–130	$3 \times 69,692,004$
SGG	$V_{XX}, V_{YY}, V_{ZZ}, V_{XZ}$	41 gapless segments	2–250	$4 \times 67,305,785$
REG	Zonal coefficients	–	$m < \theta_0 l$	6,866
REG	High-degree coefficients	–	180–250	27,208
EGM_TIM_RL05	SST, SGG, REG	11/2009–10/2013	2–280	765,504,101
SST	Short arcs, 3-D positions	35 min arcs	2–150	$3 \times 108,754,709$
SGG	$V_{XX}, V_{YY}, V_{ZZ}, V_{XZ}$	87 gapless segments	2–280	$4 \times 109,799,264$
REG	Zonal coefficients	–	$m < \theta_0 l$	8,644
REG	High-degree coefficients	–	201–280	34,274

2.1.3. Stochastic Prior Information

Due to the polar gap, and to a minor extent, due to the downward continuation within the estimation process, the solution of the NEQs is an ill-posed problem. To stabilize the solution and to improve the cut-off behavior of the SH expansion, stochastic prior information was introduced. Selected coefficients were constrained toward zero via the introduction of pseudoobservations

$$x_i = 0, \quad \text{with } \sigma_{x_i} = \frac{10^{-5}}{l^2}, \quad x_i \in \{c_{lm}, s_{lm}\} \tag{8}$$

where σ_{x_i} means the standard deviation derived from Kaula's rule of thumb [cf. *Kaula*, 1966, p. 98].

Two independent regularization matrices were set up. The first regularization matrix $\mathbf{N}_{\mathrm{PG}}$ serves for the stabilization of the coefficients affected by the polar gap (near-zonal coefficients), whose entries are

$$\mathbf{N}_{\mathrm{PG}}(i,i) = 10^{10} l^4, \text{ if } m < m_{\max} = \lceil \theta_0 l \rceil \tag{9}$$

where m is the SH order and l the SH degree of the parameter associated with the position i in the parameter vector $\mathbf{x}$. The maximal order affected by the polar gap [*van Gelderen and Koop*, 1997] is $m_{\max}$ and θ_0 is the opening angle of the polar gap in radians (≈ 0.11 for GOCE).

The second regularization matrix $\mathbf{N}_{\mathrm{HD}}$ stabilizes the coefficients of higher degrees ($l > 200$) and improves the signal-to-noise ratio. This regularization matrix has the entries

$$\mathbf{N}_{\mathrm{HD}}(i,i) = 10^{10} l^4, \text{ if } m > m_{\max} = \lceil \theta_0 l \rceil \text{ and } l > 200. \tag{10}$$

Whereas the weights w_{HD} for the high-degree regularization was estimated by VCE ($w_{\mathrm{HD}} = 0.7535$), the weight w_{PG} for the polar-gap-related zonal regularization was determined empirically (a stronger regularization was required to improve the cutoff behavior at lower SH degrees) with values $w_{\mathrm{PG}} = 4.0$ for degrees above 180, $w_{\mathrm{PG}} = 9.0$ for degrees 11 to 180.

2.2. Processed Data

Since the start of the mission on 17 March 2009 and its end in November 2013, 1270 effective measurement days (excluding satellite outages/maneuvers) were collected at different satellite altitudes with a 1 Hz sampling. Toward the end of the mission, the satellite orbit was lowered from the nominal mean altitude of 255 km down to a mean altitude of 224 km to improve the signal-to-noise ratio for the high-frequency gravity field signal (included in the RL05 solution). $4 \times 109,799,264$ gravity gradient records and 108,754,709 3-D positions were used to estimate EGM_TIM_RL05. In total 765×10^6 observations were processed to estimate 78,957 unknown gravity field parameters. Due to the better signal-to-noise ratio at higher spatial resolution (caused by lowering the altitude and by the increased data volume), the resolution was increased to d/o 280 (71.5 km) in comparison to former releases. For the analysis, especially for the filtering, the data were partitioned into gapless segments. For every segment of the time series, an individual decorrelation filter was adjusted. For RL05, the data were partitioned into 87 segments, thus $4 \times 87 = 348$ filters were iteratively refined. Table 1 summarizes the processed data in comparison to former releases.

3. The Solution EGM_TIM_RL05

In addition to the SH coefficients, their full covariance matrix (23 GB for a triangle of the symmetric matrix) is an essential part of the EGM_TIM_RL05 model. Due to the applied processing scheme, the derived covariance matrix realistically reflects the model uncertainties; no a posteriori calibration with respect to external data sets was applied. This section summarizes some characteristics of the model and describes comparisons with independent gravity field models. The detailed and specific validation of the model is not part of this paper and will be performed in the future using independent methods and data sets as done for the previous GOCE models by *Gruber et al.* [2011], *Hirt et al.* [2011], *Rexer et al.* [2014], *Becker et al.* [2014], and *Voigt and Denker* [2014].

3.1. Solution Characteristics in the Frequency Domain

Degree variances [see, e.g., *Heiskanen and Moritz*, 1993, p. 259] are commonly used to characterize an SH model by its spectral behavior depending on its SH degree,

$$\sigma(l)^2 = \sum_{m=0}^{l} \left(c_{lm}^2 + s_{lm}^2 \right). \tag{11}$$

For GOCE-only models, the near-zonal coefficients can be excluded by defining

$$\bar{\sigma}(l)^2 = \sum_{m=0}^{l} \begin{cases} c_{lm}^2 + s_{lm}^2 & \text{if } m > \lceil \theta_0 l \rceil \\ 0 & \text{otherwise} \end{cases}, \tag{12}$$

to derive a quantity which is less sensitive to the polar gap. One may replace c_{lm} and s_{lm} in (11) and (12) by coefficient differences of two models to be compared to each other. This gives difference degree variances, which may be considered as an empirical error estimate if the differences are taken with respect to a superior reference model. Furthermore, the formal error estimate of a model in terms of degree variances can be computed by replacing c_{lm} and s_{lm} with the estimated standard deviations $\sigma_{c_{lm}}$ and $\sigma_{s_{lm}}$ of the SH coefficients.

The plots of Figure 1 show various comparisons in terms of degree variances for the new model EGM_TIM_RL05 (cf. equation (12)). The first analysis in Figure 1a yields a comparison of the final GOCE solution with its two different contributors, the SST-only solution EGM_TIM_RL05_SST and the SGG-only solution EGM_TIM_RL05_SGG. Both partial solutions were obtained by solving the respective NEQs individually for the groups r and g in equation (2). The reference model in this plot is the GRACE-only ITG-Grace2010s model [cf. *Kurtenbach et al.*, 2009; *Mayer-Gürr et al.*, 2010a, 2010b]. Since state-of-the-art GRACE models are assumed to be more accurate than GOCE-only models up to at least SH degree 50, the degree variance differences to ITG-Grace2010s are taken as a measure for the long-wavelength error of the GOCE model. Up to SH degree 13, the SST-only solution and the final solution coincide. For SH degrees higher than 40, the SGG contribution dominates the combination of SGG and SST, since the blue and the green curves are more or less identical. However, some contribution by SST is visible up to degree 90. This can be seen in the formal error estimates (dashed lines) where the blue curve is below the green curve. Figure 1a further shows that

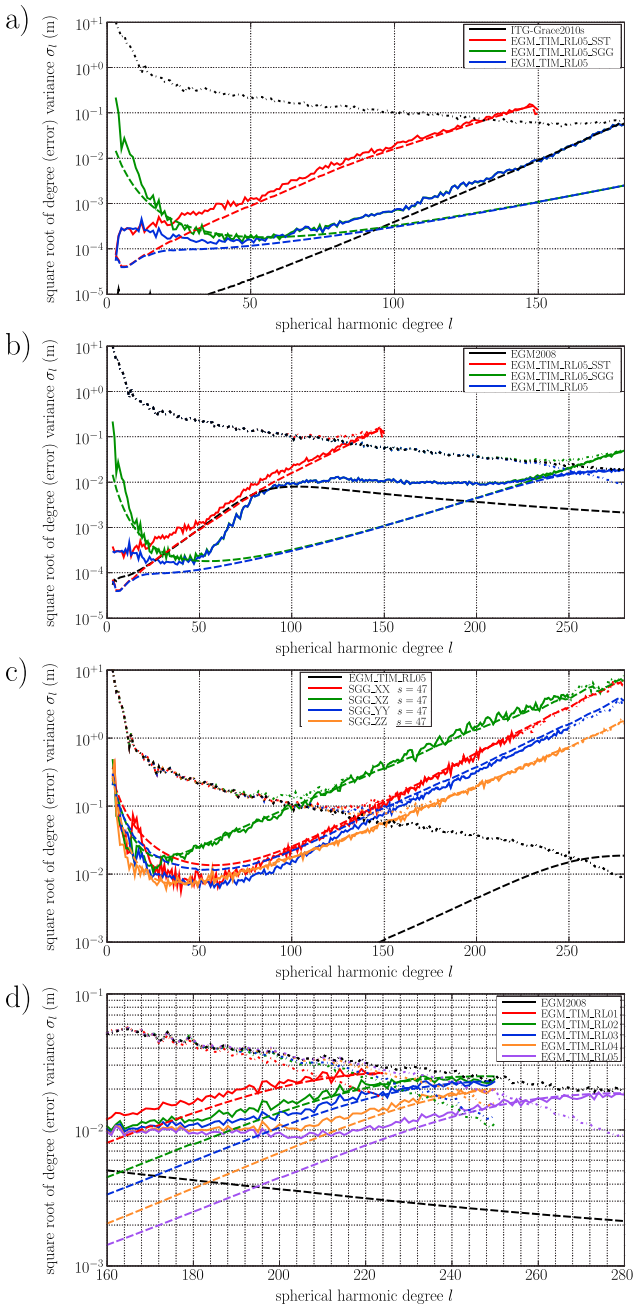

Figure 1. Characteristics of the EGM_TIM_RL05 solution by comparison of degree variances in terms of geoid heights. In these four plots, signal curves (dash-dotted lines), differences to the respective reference model (solid lines), and formal error estimates (dashed lines) are shown. (a) For the low degrees, given is a comparison of EGM_TIM_RL05 and of its contributors SGG and SST with ITG-Grace2010s. (b) For the higher degrees, shown is the comparison with EGM2008. (c) To demonstrate consistency, component-wise subsolutions for a short segment are compared with the final solution EGM_TIM_RL05. (d) The progress along the GOCE mission is demonstrated, comparing all five EGM_TIM_RL0* solutions to EGM2008 for the higher degrees, showing the decreasing noise and the increasing signal for the higher degrees.

errors in the GRACE solution start to become significant beyond degree 60. Within the degree range 60 to 120, the GRACE model and the final GOCE solution are of comparable accuracy levels, and both error budgets significantly contribute to the coefficient difference. Beyond degree 120, the errors of the GRACE model are larger than those of GOCE, since the differences between GRACE and GOCE are almost identical. It can be seen for the very low degrees 2–30 that the formal errors of EGM_TIM_RL05 are estimated slightly too optimistic since the differences to ITG-Grace2010s are larger in this degree range. This can be explained by systematic errors in the kinematic orbits [*Bock et al.*, 2014], which are reduced but not completely eliminated in the applied processing strategy (cf. section 2.1.1).

To evaluate the behavior in the higher degrees, a comparison with the combined high-resolution model EGM2008 [*Pavlis et al.*, 2012] is performed, which (i) is independent of GOCE (as it was generated before the GOCE mission) and (ii) has been compiled from the worldwide largest collection of terrestrial gravity field data. Figure 1b shows spectral comparisons of EGM_TIM_RL05, EGM_TIM_RL05_SST, and EGM_TIM_RL05_SGG to EGM2008. One can assume for a global mean that EGM_TIM_RL05 is more accurate than EGM2008 in the degree range 50–200. Up to around degree 220, the signal power of EGM_TIM_RL05 is almost the same as that of EGM2008 (notice the green and black dash-dotted lines). Beyond degree 220 the error in the GOCE model dominates the difference. Starting from degree 225, the higher degrees cannot be properly estimated and are therefore constrained toward zero by the Kaula regularization according to (10). Nevertheless, there is still some signal at that degree range, which could be estimated from the GOCE observations. The spectral signal-to-noise ratio for the unconstrained solution (SGG only) is 1.0 at degree 254 (79 km).

Figure 1c indicates that the formal error estimates as provided together with the solution are of a realistic order of magnitude. SGG-only subsolutions for each tensor component of a single segment (period 1–19

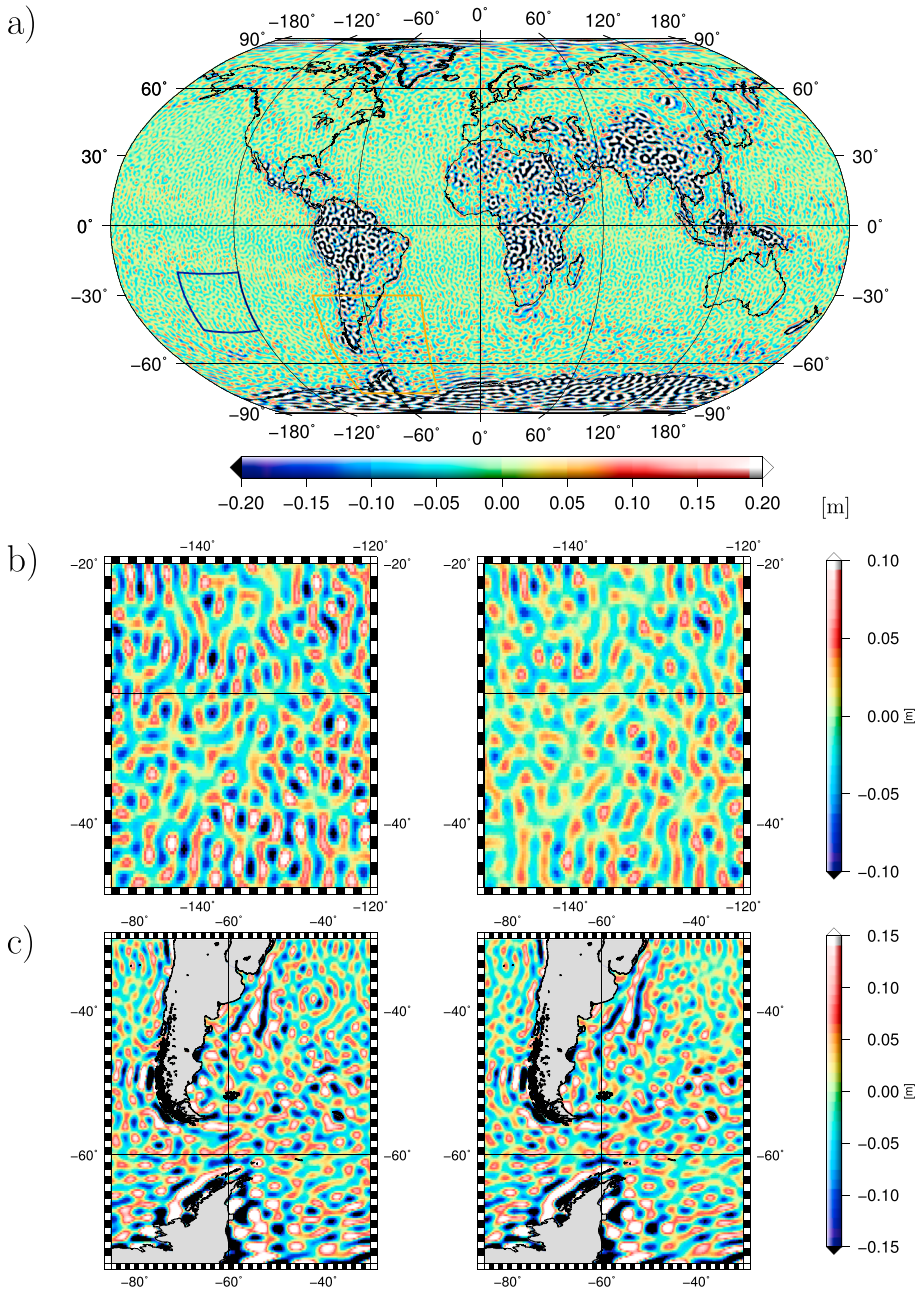

Figure 2. Geoid height differences (meter) of time-wise models with respect to the EGM2008 at spherical harmonic degree 200. (a) The global differences between EGM2008 and EGM_TIM_RL05. (b) A local focus on the open South Pacific, where EGM2008 is assumed to be of superior accuracy. The left shows the difference of the older EGM_TIM_RL04 to EGM2008, and the right shows the difference of EGM_TIM_RL05 to EGM2008. These pictures demonstrate the gain in accuracy from RL04 to RL05. (c) Same as Figure 2b but for an area where the gain of the GOCE models with respect to EGM2008 is highlighted. A coastal area, in the south of South America, with smaller currents at the east coast. Significant differences from both releases to EGM2008 occur, which indicate unmodeled or mismodeled geoid signal in EGM2008. This signal is captured by the GOCE models.

July 2012, 1.6×10^6 observations) are compared to the final EGM_TIM_RL05 solution. As 275 times more observations are used in EGM_TIM_RL05, it is assumed to be a dominant reference solution which is much more accurate than the subsolution from the short period and the single SGG component. The empirically estimated errors from coefficient differences (solid lines) properly correspond to the formal error estimates derived from the covariance matrix of the SH coefficients (dashed lines). For the lower degrees, the formal errors seem to be rather too pessimistic.

Finally, Figure 1d shows the improvement along the five releases of the time-wise models, again as a comparison to EGM2008. The figure shows the higher degrees where the gain in accuracy is visibly best. The increased signal is visible from release to release (dash-dotted lines) and gets closer and closer to the full EGM2008 signal in the degree range 220–280 (because the used terrestrial and altimetry data sets in EGM2008 are of higher accuracy in this degree range). The corresponding decreasing error estimates reflect the gain in accuracy.

3.2. Comparison to EGM2008 in the Space Domain

Figure 2 shows geoid height differences between EGM_TIM_RL05 and EGM2008, computed from the SH coefficients of both models up to d/o 200. The global view (cf. Figure 2a) is dominated by large systematic differences over land. These differences are supposed to be systematic errors in EGM2008 mainly in such regions where no, or low-quality, terrestrial data entered the computation of EGM2008 [*Pavlis et al.*, 2012; *Pail et al.*, 2011a; *Bruinsma et al.*, 2013].

However, restricting the comparison to local areas, e.g., to the open South Pacific (green box in Figure 2a), where the dynamic ocean topography (DOT) is smooth, it can be assumed that EGM2008 has a high quality. Over the oceans, EGM2008 was determined from decades of altimetric sea surface height observations [e.g., *Andersen and Knudsen*, 2009] at that spatial resolution. In areas, where the DOT is smooth, the separation of the sea surface height into the geoid and the DOT is expected to be more precise than in other areas. We assume that in such carefully selected local areas, EGM2008 is more accurate than the GOCE models. Figure 2b shows a zoom into that area for EGM_TIM_RL04 (left) and EGM_TIM_RL05 (right). From Release 4 to 5, a significant reduction of the difference is clearly visible, which demonstrates the improvement in the model quality. For this particular region, the root-mean-square values of the geoid height differences between EGM2008 and both GOCE models decrease from 4.1 cm for EGM_TIM_RL04 to 2.8 cm for EGM_TIM_RL05. Propagating the covariance matrix of the SH coefficients to geoid height errors for that region, a mean error of the model of 4.0 cm for EGM_TIM_RL04 and 2.8 cm for EGM_TIM_RL05 is derived. (Note that this mean error does not include the EGM2008 error budget.) Thus, the formal error estimates and empirical comparisons to EGM2008 in specific regions show a good agreement. For the region selected here, the conclusions are twofold: First, EGM2008 has high quality and is consistent with the GOCE models—within the error level of the GOCE model. Second, the provided covariance matrix realistically reflects the error of the model, as the propagated error is confirmed by the empirical comparison to EGM2008.

Investigating spatially restricted areas, where altimetric observations are known to be less accurate (i.e., coastal areas and regions at high/low latitudes of low altimetry coverage), significant differences become visible (see Figure 2a), which are larger than the error levels of the GOCE model. As the gravity fields determined from GOCE data have a homogeneous error structure in the spatial domain [e.g., *Pail et al.*, 2011a; *Brockmann et al.*, 2013], the GOCE model uncertainties are independent of the signal and are not geographically correlated. Thus, it can be certainly concluded that the visible spatial differences are errors or uncertainties within EGM2008. Furthermore, larger differences are visible in such ocean areas where the DOT is rough and ocean currents occur. Within these areas, the separation process of the altimetric observations into geoid and DOT is challenging, but one should keep in mind that this subject is one of the main goals of the GOCE gravity field models [e.g., *ESA*, 1999; *Rummel et al.*, 2002]. In this context, the gain of the GOCE mission for oceanographic applications can be impressively demonstrated in coastal areas and such ocean areas where the DOT is not smooth and where strong currents occur, e.g., along the Antarctic Circumpolar Current (see north of Antarctica in the global plot of Figure 2a). Patterns of larger geoid height differences between EGM2008 and EGM_TIM_RL05 are clearly visible. There is no reason for the globally homogeneous and consistent GOCE model to be less accurate in this area. Therefore, one can conclude that geoid errors in EGM2008 are the reasons for these increased differences. In contrast to the "smooth" areas, a detailed view into areas where the ocean is known to not be smooth (around currents) and into coastal areas is given in Figure 2c. This figure shows a selected region southeast of South America, around the smaller Brazil and Falkland currents. Large systematic differences occur in these areas, which become better pronounced with increasing GOCE version number, e.g., from EGM_TIM_RL04 to EGM_TIM_RL05. These differences are obviously caused by unmodeled or mismodeled geoid signal in EGM2008. These regions along the Antarctic Circumpolar Current and southeast of South America are examples for areas where GOCE significantly improves the marine geoid.

4. Summary and Conclusions

EGM_TIM_RL05 is the first global gravity field model purely based on the data from the entire GOCE mission. This model based on the time-wise approach is one of ESA's official GOCE gravity field releases and was computed without any other, non-GOCE measurements. Thus, it is independent of other gravity field models and gravity data sets. Current estimates of the global mean accuracy are of about 2.4 cm at a spatial scale of 100 km (and below 10 cm at 80 km resolution) outside the polar regions, corresponding to 0.69 mGal (and 3.37 mGal, respectively) in terms of gravity anomalies. In contrast to models based on a combination of data from several gravity satellite missions (and terrestrial data), it is not of highest accuracy, but it reflects the Earth's gravity field as observed by the GOCE satellite. Although the very long wavelengths and the low-order coefficients are not competitive with those of models that include GRACE and SLR observations, this latest time-wise GOCE model is of high quality in the short wavelengths and outside the polar regions. EGM_TIM_RL05 demonstrates the progress of GOCE for the global gravity field recovery. A global homogeneous solution was derived, whose error structure (except for the polar gaps) is not correlated to geographic features. For example, the separation of altimetric sea surface height measurements into geoid and DOT will be strongly supported by this, for the time being, final global GOCE model. It is very well suited, for the estimation of the DOT [e.g., *Bingham et al.*, 2011; *Becker et al.*, 2014], as a background model for local geoid computations or height unification [e.g., *Rummel*, 2013] or for the estimation of combined models [e.g., *Pail et al.*, 2010]. For that purpose, unconstrained NEQs or covariance matrices can be requested from the authors. EGM_TIM_RL05 and its associated full covariance matrix was published together with other official Release 5 products via ESA's GOCE Virtual Online Archive and via the ICGEM data base (the sole models are available on http://icgem.gfz-potsdam.de/ICGEM/).

Acknowledgments

Contributions (data preparation, distribution, and preprocessing) by all members of the GOCE High-level Processing Facility are gratefully acknowledged. (The work by all contributors is summarized in the related special issue in the *Journal of Geodesy* [*Rummel et al.*, 2011].) This work was financially supported by ESA GOCE HPF (main contract 18308/04/NL/MM). The used GOCE L1B and L2 data are freely provided by ESA via the ESA GOCE Virtual Archive (http://eo-virtual-archive1.esa.int/). Most of the computations were performed on the JUROPA supercomputer at FZ Jülich. The computing time was granted by the John von Neumann Institute for Computing (project HBN15). Some computations were performed on the new cluster at the University of Bonn financed via a DFG Forschungsgroßgeräteantrag (INST 217/747-1 FUGG). The Open Source software packages GMT (Generic Mapping Tools) [*Wessel and Smith*, 1998] and OCTAVE [*Eaton et al.*, 2009] are gratefully acknowledged. We would like to thank the Editor and the two anonymous reviewers for their comments and discussion which helped a lot to improve the quality of the manuscript.

Eric Calais thanks two anonymous reviewers for their assistance in evaluating this paper.

References

Andersen, O. B., and P. Knudsen (2009), DNSC08 mean sea surface and mean dynamic topography models, *J. Geophys. Res.*, *114*, C11001, doi:10.1029/2008JC005179.

Baur, O., H. Bock, E. Höck, A. Jäggi, S. Krauss, T. Mayer-Gürr, T. Reubelt, C. Siemes, and N. Zehentner (2014), Comparison of GOCE-GPS gravity fields derived by different approaches, *J. Geod.*, *88*, 959–973, doi:10.1007/s00190-014-0736-6.

Becker, S., J. M. Brockmann, and W.-D. Schuh (2014), Mean dynamic topography estimates purely based on GOCE gravity field models and altimetry, *Geophys. Res. Lett.*, *41*, 2063–2069, doi:10.1002/2014GL059510.

Bingham, R. J., P. Knudsen, O. B. Andersen, and R. Pail (2011), An initial estimate of the North Atlantic steady-state geostrophic circulation from GOCE, *Geophys. Res. Lett.*, *38*, L01606, doi:10.1029/2010GL045633.

Bock, H., A. Jäggi, G. Beutler, and U. Meyer (2014), GOCE: Precise orbit determination for the entire mission, *J. Geod.*, *88*, 1047–1060, doi:10.1007/s00190-014-0742-8.

Brockmann, J. M., E. Höck, I. Krasbutter, T. Mayer-Gürr, R. Pail, W.-D. Schuh, and N. Zehentner (2013), Performance of the fourth generation GOCE time-wise Earth gravity field model, Geophysical Research Abstracts EGU2013-9401 paper presented at EGU General Assembly 2013, Vienna, 7–12 April.

Bruinsma, S. L., C. Förste, O. Abrikosov, J.-C. Marty, M.-H. Rio, S. Mulet, and S. Bonvalot (2013), The new ESA satellite-only gravity field model via the direct approach, *Geophys. Res. Lett.*, *40*, 3607–3612, doi:10.1002/grl.50716.

Bruinsma, S. L., C. Förste, O. Abrikosov, J.-M. Lemoine, J.-C. Marty, S. Mulet, M.-H. Rio, and S. Bonvalot (2014), ESA's satellite-only gravity field model via the direct approach based on all GOCE data, *Geophys. Res. Lett.*, *41*, doi:10.1002/2014GL062045.

Dach, R., E. Brockmann, S. Schaer, G. Beutler, M. Meindl, L. Prange, H. Bock, A. Jäggi, and L. Ostini (2009), GNSS processing at CODE: Status report, *J. Geod.*, *83*(3–4), 353–365, doi:10.1007/s00190-008-0281-2.

Eaton, J. W., D. Bateman, and S. Hauberg (2009), *GNU Octave Version 3.0.1 Manual: A High-Level Interactive Language for Numerical Computations*, CreateSpace Indep. Publ. Platform, North Charleston, S. C., ISBN 1441413006.

EGG-C (2010), *GOCE standards 3.2, GO-TN-HPF-GS-011*.

ESA (1998), *The Earth Explores—The Science and Research Elements of ESA's Living Planet Programme, ESA SP*, vol. 1227, ESA Publ. Div., Noordwijk, Netherlands.

ESA (1999), *The Four Candidate Earth Explorer Core Missions—Gravity Field and Steady-State Ocean Circulation, ESA SP*, vol. 1233, ESA Publ. Div., Noordwijk, Netherlands.

Farahani, H. H., P. Ditmar, R. Klees, X. Liu, Q. Zhao, and J. Guo (2013), The static gravity field model DGM-1S from GRACE and GOCE data: Computation, validation and an analysis of GOCE mission's added value, *J. Geod.*, *87*(9), 843–867, doi:10.1007/s00190-013-0650-3.

Floberghagen, R., M. Fehringer, D. Lamarre, D. Muzi, B. Frommknecht, C. Steiger, J. Pineiro, and A. da Costa (2011), Mission design, operation and exploitation of the gravity field and steady-state ocean circulation explorer mission, *J. Geod.*, *85*(11), 749–758, doi:10.1007/s00190-011-0498-3.

Förste, C., et al. (2008), The GeoForschungsZentrum Potsdam/Groupe de Recherche de Geodesie Spatiale satellite-only and combined gravity field models: EIGEN-GL04S1 and EIGEN-GL04C, *J. Geod.*, *82*(6), 331–346, doi:10.1007/s00190-007-0183-8.

Fritsche, M., R. Dietrich, C. Knöfel, A. Rülke, S. Vey, M. Rothacher, and P. Steigenberger (2005), Impact of higher-order ionospheric terms on GPS estimates, *Geophys. Res. Lett.*, *32*, L23311, doi:10.1029/2005GL024342.

Frommknecht, B., D. Lamarre, M. Meloni, A. Bigazzi, and R. Floberghagen (2011), GOCE level 1b data processing, *J. Geod.*, *85*(11), 759–775, doi:10.1007/s00190-011-0497-4.

Gruber, T., P. N. A. M. Visser, C. Ackermann, and M. Hosse (2011), Validation of GOCE gravity field models by means of orbit residuals and geoid comparisons, *J. Geod.*, *85*(11), 845–860, doi:10.1007/s00190-011-0486-7.

Hausleitner, W. (1995), Orbit and SGG data simulations, *Tech. rep.*, ESA-Project CIGAR III / Phase 2, WP 221, Final-Report, Part 1, Technical Univ. Graz, Graz, Austria.

Heiskanen, W. A., and H. Moritz (1993), *Physical Geodesy* reprint ed., Inst. of Phys. Geod., Tech. Univ. Graz, Graz, Austria.
Hirt, C., T. Gruber, and W. E. Featherstone (2011), Evaluation of the first GOCE static gravity field models using terrestrial gravity, vertical deflections and EGM2008 quasigeoid heights, *J. Geod.*, *85*(10), 723–740, doi:10.1007/s00190-011-0482-y.
Hoque, M. M., and N. Jakowski (2008), Estimate of higher order ionospheric errors in GNSS positioning, *Radio Sci.*, *43*, RS5008, doi:10.1029/2007RS003817.
Kaula, W. M. (1966), *Theory of Satellite Geodesy: Applications of Satellites to Geodesy* reprint ed., Dover, Mineola, New York.
Koch, K. R. (1999), *Parameter Estimation and Hypothesis Testing in Linear Models*, 2nd ed., Springer, Berlin, Heidelberg.
Koch, K. R., and J. Kusche (2002), Regularization of geopotential determination from satellite data by variance components, *J. Geod.*, *76*(5), 259–268, doi:10.1007/s00190-002-0245-x.
Krasbutter, I., J. M. Brockmann, B. Kargoll, and W.-D. Schuh (2011), Stochastic model refinements for GOCE gradiometer data, in *Observation of the System Earth from Space, Geotechnologien Sci. Rep.*, vol. 17, edited by U. Münch and W. Dransch, pp. 70–76, Koordinierungsbüro Geotechnologien, Potsdam.
Kurtenbach, E., T. Mayer-Güerr, and A. Eicker (2009), Deriving daily snapshots of the Earth's gravity field from GRACE l1b data using Kalman filtering, *Geophys. Res. Lett.*, *36*, L17102, doi:10.1029/2009GL039564.
Mayer-Gürr, T. (2006), Gravitationsfeldbestimmung aus der Analyse kurzer Bahnbögen am Beispiel der Satellitenmissionen CHAMP und GRACE, PhD thesis, Univ. of Bonn, Bonn, Germany.
Mayer-Gürr, T., A. Eicker, E. Kurtenbach, and K.-H. Ilk (2010a), ITG-GRACE: Global static and temporal gravity field models from GRACE data, in *System Earth via Geodetic-Geophysical Space Techniques*, edited by F. Flechtner et al., pp. 159–168, Springer, Berlin, Heidelberg, doi:10.1007/978-3-642-10228-8_13.
Mayer-Gürr, T., E. Kurtenbach, and A. Eicker (2010b), ITG-Grace2010: The new GRACE gravity field release computed in Bonn, Geophysical Research Abstracts EGU2010-2446 paper presented at EGU General Assembly 2010, held 2–7 May, 2010 in Vienna, Austria, p. 2446.
Mayer-Gürr, T., et al. (2012), The new combined satellite-only model GOCO03S, paper presented at International Symposium on Gravity, Geoid and Height Systems (GGHS2012), IAG Symposium Venice, Italy.
Migliaccio, F., M. Reguzzoni, A. Gatti, F. Sansò, and M. Herceg (2011), A GOCE-only global gravity field model by the space-wise approach, in *Proceedings of the 4th International GOCE User Workshop, 31 March–1 April, 2011*, edited by L. Ouwehand, p. 8, ESA Publ. SP-696, Munich, Germany.
Pail, R., and G. Plank (2002), Assessment of three numerical solution strategies for gravity field recovery from GOCE satellite gravity gradiometry implemented on a parallel platform, *J. Geod.*, *76*(8), 462–474, doi:10.1007/s00190-002-0277-2.
Pail, R., B. Metzler, B. Lackner, T. Preimesberger, E. Höck, W.-D. Schuh, H. Alkhatib, C. Boxhammer, C. Siemes, and M. Wermuth (2006), GOCE gravity field analysis in the framework of HPF: Operational software system and simulation results, in *Proceedings of the 3rd International GOCE User Workshop*, edited by K. Fletcher, pp. 249–256, ESA Publ. SP-627, Frascati, Italy.
Pail, R., et al. (2010), Combined satellite gravity field model GOCO01S derived from GOCE and GRACE, *Geophys. Res. Lett.*, *37*, L20314, doi:10.1029/2010GL044906.
Pail, R., et al. (2011a), First GOCE gravity field models derived by three different approaches, *J. Geod.*, *85*(11), 819–843, doi:10.1007/s00190-011-0467-x.
Pail, R., H. Goiginger, W.-D. Schuh, E. Höck, J.-M. Brockmann, T. Fecher, D. Rieser, I. Krasbutter, and T. Mayer-Gürr (2011b), GOCE-only gravity field models derived from 8 months of GOCE data, in *Proceedings of the 4th International GOCE User Workshop*, edited by K. Fletcher, ESA Publ. SP-696, Munich, Germany.
Pavlis, N. K., S. A. Holmes, S. Kenyon, and J. K. Factor (2012), The development and evaluation of the Earth Gravitational Model 2008 (EGM2008), *J. Geophys. Res.*, *117*, B04406, doi:10.1029/2011JB008916.
Plank, G. (2004), Numerical solution strategies for the GOCE mission by using cluster technologies, PhD thesis, Technical Univ. Graz, Graz, Austria.
Reigber, C., H. Lühr, and P. Schwintzer (2002), CHAMP mission status, *Adv. Space Res.*, *30*(2), 129–134, doi:10.1016/S0273-1177(02)00276-4.
Rexer, M., C. Hirt, R. Pail, and S. Claessens (2014), Evaluation of the third- and fourth-generation GOCE Earth gravity field models with Australian terrestrial gravity data in spherical harmonics, *J. Geod.*, *88*(4), 319–333, doi:10.1007/s00190-013-0680-x.
Rummel, R. (2013), Height unification using GOCE, *J. Geod. Sci.*, *2*(4), 355–362.
Rummel, R., et al. (2011), GOCE—The gravity and steady-state ocean circulation explorer, *J. Geod.*, *85*(11), 749–758.
Rummel, R., G. Balmino, J. Johannessen, P. N. A. M. Visser, and P. Woodworth (2002), Dedicated gravity field missions—Principles and aims, *J. Geodyn.*, *33*(1–2), 3–20, doi:10.1016/S0264-3707(01)00050-3.
Rummel, R., W. Yi, and C. Stummer (2011), GOCE gravitational gradiometry, *J. Geod.*, *85*(11), 777–790, doi:10.1007/s00190-011-0500-0.
Schall, J., A. Eicker, and J. Kusche (2014), The ITG-Goce02 gravity field model from GOCE orbit and gradiometer data based on the short arc approach, *J. Geod.*, *88*(4), 403–409, doi:10.1007/s00190-014-0691-2.
Schuh, W.-D. (1996), Tailored numerical solution strategies for the global determination of the Earth's gravity field, 81, Mitteilungen der geodätischen Institute der Technischen Universität Graz, Technical Univ. Graz, Graz, Austria.
Schuh, W.-D. (2003), The processing of band-limited measurements; filtering techniques in the least squares context and in the presence of data gaps, *Space Sci. Rev.*, *108*(1–2), 67–78, doi:10.1023/A:1026121814042.
Schuh, W.-D., J. M. Brockmann, B. Kargoll, I. Krasbutter, and R. Pail (2010), Refinement of the stochastic model of GOCE scientific data and its effect on the in-situ gravity field solution, in *Proceedings of ESA Living Planet Symposium*, edited by H. Lacoste-Francis, ESA Publ. SP-686, Bergen, Norway.
Shako, R., C. Förste, O. Abrykosov, S. Bruinsma, J.-C. Marty, J.-M. Lemoine, F. Flechtner, K.-H. Neumayer, and C. Dahle (2014), EIGEN-6C: A high-resolution global gravity combination model including GOCE data, in *Observation of the System Earth From Space—CHAMP, GRACE, GOCE and Future Missions, Advanced Technologies in Earth Sciences*, edited by F. Flechtner et al., pp. 155–161, Springer, Berlin, Heidelberg, doi:10.1007/978-3-642-32135-1_20.
Siemes, C. (2008), Digital filtering algorithms for decorrelation within large least squares problems, PhD thesis, Institute of Geodesy and Geoinformation, Univ. of Bonn, Bonn, Germany.
Stummer, C., C. Siemes, R. Pail, B. Frommknecht, and R. Floberghagen (2012), Upgrade of the GOCE level 1b gradiometer processor, *Adv. Space Res.*, *49*(4), 739–752, doi:10.1016/j.asr.2011.11.027.
Tapley, B. D., S. Bettadpur, J. C. Ries, P. F. Thompson, and M. M. Watkins (2004), GRACE measurements of mass variability in the Earth system, *Science*, *305*(5683), 503–505, doi:10.1126/science.1099192.
van Gelderen, M., and R. Koop (1997), The use of degree variances in satellite gradiometry, *J. Geod.*, *71*(6), 337–343, doi:10.1007/s001900050101.

Voigt, C., and H. Denker (2014), Regional validation and combination of GOCE gravity field models and terrestrial data, in *Observation of the System Earth From Space—CHAMP, GRACE, GOCE and Future Missions*, edited by F. Flechtner et al., pp. 139–145, Springer, Berlin, Heidelberg, doi:10.1007/978-3-642-32135-1_18.

Wessel, P., and W. H. F. Smith (1998), New, improved version of generic mapping tools released, *Eos Trans. AGU*, *79*(47), 579–579, doi:10.1029/98EO00426.

Witchayangkoon, B. (2000), *Elements of GPS Precise Point Positioning*, Univ. of Maine, Orono, Maine.

Yi, W. (2012), An alternative computation of a gravity field model from GOCE, *Adv. Space Res.*, *50*(3), 371–384, doi:10.1016/j.asr.2012.04.018.

Yi, W., R. Rummel, and T. Gruber (2013), Gravity field contribution analysis of GOCE gravitational gradient components, *Stud. Geophys. Geod.*, *57*(2), 174–202, doi:10.1007/s11200-011-1178-8.

Zehentner, N., and T. Mayer-Gürr (2012), New approach to estimate time variable gravity fields from high-low satellite tracking data, in *Proceedings of the International Symposium on Gravity, Geoid and Height Systems (GGHS2012), International Association of Geodesy Symposia*, vol. 141, edited by U. Marti, p. 218, Springer, Berlin, Heidelberg.

Zehentner, N., and T. Mayer-Gürr (2013), A new approach for precise orbit determination based on raw GNSS measurements, paper presented at European Geosciences Union General Assembly 2013, *Geophys. Res. Abstr.*, *15*, EGU2013-5169-1, Vienna.

Zehentner, N., and T. Mayer-Gürr (2014), Gravity variations from precise LEO orbits of GRACE and GOCE, paper presented at European Geosciences Union General Assembly 2014, *Geophys. Res. Abstr.*, *16*, EGU2014-6018, Vienna.